Automation of a Teleoperated Microassembly Desktop Station Supervised by Virtual Reality

Antoine Ferreira, Jean-Guy Fontaine, and Shigeoki Hirai

Abstract: We proposed a concept of a desktop micro device factory for visually servoed teleoperated microassembly assisted by a virtual reality (VR) interface. It is composed of two micromanipulators equipped with micro tools operating under a light microscope. First, a manipulator control method for the micro object to follow a planned trajectory in pushing operation is proposed under vision based-position control. Then, we present the cooperation control strategy of the micro handling operation under vision-based force control integrating a sensor fusion framework approach. A guiding-system based on virtual micro-world exactly reconstructed from the CAD-CAM databases of the real environment being considered is presented for the imprecisely calibrated micro world. Finally, some experimental results of microassembly tasks performed on millimeter-sized components are provided.

Keywords: microrobotics, visual force/position feedback, virtual reality, microassembly.

I. Introduction

The recent development of microelectromechanical systems (MEMS) moves toward smaller components and increasingly complex microstructures thus requiring sophisticated micro-manipulation techniques. Furthermore, the future mass production of MEMS will require fully automatic assembly of hybrid components with very limited human interaction in order to preserve potential economic benefits. With these developments on the horizon, the need for sophisticated micro-factories becomes real and large for the automatic assembly and testing of prototype devices. Up to now, new systems of static "desktop micro- and nano-manipulation stations" [1]-[2] or mobile "flexible autonomous microrobots"[3]-[5] have been reported. In view of the emerging applications in this field, we have demonstrated practically the feasibility of such a kind of desktop micro device factory integrating static desktop working cells [6], cooperating with mobile microrobots such as multidegree of freedom mobile micromanipulators equipped with micro-tools [7], micropositioning systems [8] and flexible microconveyers [9]. In such microrobotic applications where the remote world is partially modelled and the situations are to some extent predicable, tasks can be performed in part autonomously by the microrobotic systems [10]. Human intervention is needed only in failure or unpredicted situations. This work proposes a new automated microfactory concept which integrates different functions, i.e. handling, conveying, manipulation and assembly of micro sized objects. A key aspect of the proposed method concern the integration of a virtual microworld with visual servoing strategies to perform off-line programming of the automatic task in the real microworld. Automated microfactory floor microdevices, such as micromanipulators, microconveyers and turntables, can be programmed off-line based on CAD-CAM data for the microparts being processed. A schematic view of the teleoperated micromanipulation system is presented in Fig.1. A supervisor interacts within the virtual microworld using VRML (Virtual Reality Mondeling Language) by giving high-level commands to the workcell. Firstly, we briefly present the sensor fusion framework approach that integrates an optically based force/position sensor. Then, a guiding-system based on virtual micro-world exactly reconstructed from the CAD-CAM databases of the real environment being considered is presented. Finally, some experimental results of microassembly tasks performed on millimeter-sized components are provided.

Manuscript received: Aug. 23, 2001, Accepted: Nov. 16, 2001.

Antoine Ferreira, Jean-Guy Fontaine: Laboratoire de Vision et Robotique (LVR), ENSIB, 18000, Bourges, France(antoine.ferreira@ensi-bourges.fr)

Shigeoki Hirai: Intelligent Systems Institute, AIST, Tsukuba-shi, Ibaraki 305-8568, Japan

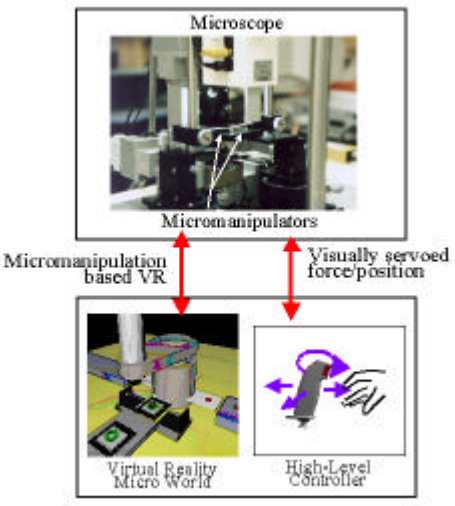

Fig. 1. Teleoperated micro assembly workcell under a microscope.

II. Microassembly system

The current configuration of the micro handling system consists of two concentrated motion micromanipulators (main and sub) equipped with a micro tool holder, a coarse motion worktable (driving with piezoelectric actuators, the movable ranges: 30×30×30mm), a multidegree of freedom fine positioning system (driving with piezoelectric actuators, the movable ranges: 100×100×100μm). The orientation of the end-effectors can also be changed by two accurate ultrasonic motors. A reflecting light-type Optical Microscope (OM) is used as a top-view vision sensor. A high-definition camera on the OM is connected to the Matrox Co. Frame-grabber which enables real-time image viewing of the micro world on the teleoperator interface. Our system has been designed so that: i)

the degrees of freedom (d.o.f.) are divided between two arms, allowing better operation and flexibility under microscope, ii) the concentrated motion micromanipulators are so designed that all rotational centers of the degrees of freedom coincide each other at the tool tips. The operating principle of the microassembly task is decomposed in different steps as it is shown in Fig.2. The *tool carrier* (sub micromanipulator) allows to transport a millimeter-sized object, using stepping micro pushing operation, to its final position before to be handled. Variations in the friction force at the object-support interface are the main cause of disturbances that appears particularly during the translational push. This results in a unknown change in object orientation. In order to correct the object orientation, cooperative control commands are sent to the micro pusher and the piezoelectric worktable. The left arm is the *tool holder* (main micromanipulator). It allows to handle the small object with a stable gripping under force control feedback. Once the micro-object is handled, microassembly task can thus be initiated.

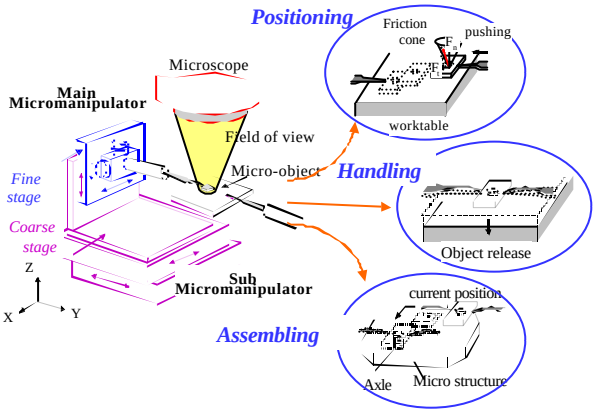

Fig. 2. Sequencing of the different operating tasks.

III. Visually servoed position/force control

1. Micropositioning control using pushing operation

The *carrier tool* is controlled in such a way to transport the micro object to its final location using pushing operation. In the study of pushing, the relation between the motion of the pushed object and the frictional forces between the object and the support surface is important. When pushing an object, since it is difficult to control the motion of pushed object if there is slip between the object and the pusher, it is necessary to provide some means to avoid the slip. An appropriate trajectory must be planned, so that the object will be moved to the desired position and orientation. However, since there are uncertain factors, which are not considered in planning, such as changes of the friction distribution, during actual position, we need a feedback control method for pushing the object along a trajectory [11]-[12]. The major property of the propose method is to use a particular point obtained from the given friction distribution, named pseudo-center introduced by Kurisu [13]. Some simulations (Fig. 3) have been done on LISP language in order to visualize the locus of instantaneous rotation center of the object in the pushing operation, when the direction of pushing velocity at the contact point is varied.

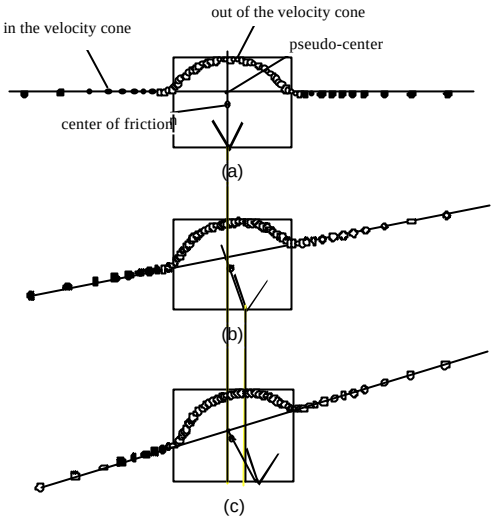

Fig. 3. Simulation of the variation of the rotation center of a rectangular shape micro-object (5mm×3mm).

Figure 3 shows example plots of rotation centers for a rectangular micro-object with uniform friction distribution when the direction of pushing velocity is changed with an increment of $\pi/50$. The difference among the Fig. 3(a-b) and (c) is the location of contact point on the object. In each figure, the region between the two thick rays at the contact point represents the velocity cone. When the direction of pushing velocity lies in this cone, the manipulator tips can push the object without any slip. This velocity cone corresponds to the friction cone, and is determined by the friction distribution of the object and the coefficient of friction between the manipulator tips and the object. The circle located at the center of the object is the centroïd of the friction distribution, called the center of friction. When the direction of velocity at the contact point goes through the center of friction, the motion of the object is a pure translation. The black dots and the white dots correspond to the rotation centers of the object motion when the direction of velocity is in the velocity cone and out of the cone, respectively. Hence only the black dots can be realized.

Accordingly, it will be possible to realize the tracking control of the object in pushing operation by applying a tracking control rule for the main micromanipulator. Indeed, Fig. 3(a) shows the ideal case for controlling the object motion, because the object can be turned both clockwise and counterclockwise without any slip between the manipulator tip and the object. On the other hand, in the case of Fig. 3(b), the object can be turned only counterclockwise. In the case of Fig. 3(c), the location of the rotation center is more limited. On the pseudo-center, the motion of the pushed object can be approximately regarded as the motion of the end-effector on its center. It is assumed that the motion of the pushed object can be regarded as the motion ${}^{U}\mathbf{v}_c$ of the main manipulator with two independent degrees of freedom on its midpoint.

$$\begin{bmatrix} \bar{v}_{0'} \\ \dot{q} \end{bmatrix} = \begin{bmatrix} \bar{v}_c \cos(a - a_0) \\ \dfrac{\bar{v}_c}{l_p} \sin(a - a_0) \end{bmatrix} = \mathbf{B}\, {}^{U}V_c \qquad (1)$$

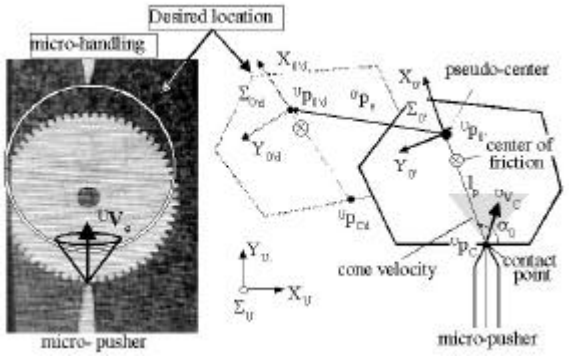

Fig. 4. Pushing-based position tracking.

Furthermore, it is considered that the desired trajectory of the object is given by the position ${}^{U}\mathbf{p}_{O'd}(t)$ and velocity ${}^{U}\dot{\mathbf{p}}_{O'd}(t)$ of the center of friction expressed in Σ_U fixed on the support, and the orientation $q_{O'd}(t)$ and rotational velocity $\dot{q}_{O'd}(t)$ of the object, ${}^{U}w_{O'd}=\left[{}^{U}\mathbf{p}_{O'd},q_{O'd}\right]^T$ and ${}^{U}\dot{w}_{O'd}=\left[{}^{U}\dot{\mathbf{p}}_{O'd},\dot{q}_{O'd}\right]^T$. It is also assumed that we can measure the position ${}^{U}\mathbf{p}_c$ and velocity ${}^{U}\mathbf{v}_c$ of the object at the contact point expressed in Σ_U, and the orientation q and rotational velocity $\dot{q}$. Let Σ_O denote the coordinate frame with its origin at the pseudo-center and its X axis parallel to the line which joins the contact point and the center of friction. These considerations allow to define the error vector of the pseudo-center expressed in Σ_O with respect to the desired trajectory defined as $e_{O'}=\left[{}^{O'}\mathbf{p}_e{}^T,q_e\right]^T$:

i) the position error vector: The position error of the pseudo-center expressed in Σ_O with respect to the desired trajectory is denoted as ${}^{O'}\mathbf{p}_e=\left[{}^{O'}x_e,{}^{O'}y_e\right]^T$. Denoting the actual position of pseudo-center expressed in Σ_U as ${}^{U}\mathbf{p}_{O'}$, the desired position as ${}^{U}\mathbf{p}_{O'd}$, and the rotational matrix from Σ_O to Σ_U as ${}^{U}\mathbf{R}_{O'}$, the error ${}^{O'}\mathbf{p}_e$ is given by :

$${}^{O'}p_e={}^{U}\mathbf{R}_{O'}^{T}\left({}^{U}p_{O'd}-{}^{U}p_{O'}\right) \tag{2}$$

ii) the orientation error: It is considered as:

$$q_e=q_d-q \tag{3}$$

Hence, we apply a differential feedback control rule [13] for determining the linear and rotational velocities of the main micromanipulator according to the position and orientation errors with respect to the desired trajectory expressed in the coordinate frame fixed on the manipulator. The adopted control rule

$$\begin{bmatrix}\bar{v}_0\\ \dot{q}\end{bmatrix}=\begin{bmatrix}\bar{v}_{O'd}\cos q_e+K_x{}^{O'}x_e\\ \dot{q}_d+\bar{v}_{O'd}\left(K_y{}^{O'}y_e+K_q\sin q_e\right)\end{bmatrix} \tag{4}$$

guarantees that the actual trajectory converges uniformly asymptotically to the desired trajectory, which means that $e_{O'}=\left[{}^{O'}p_e{}^T,q_e\right]^T$ converges to 0 as far as $\bar{v}_{O'd}>0$. The terms K_x, K_y, and K_θ are feedback parameters. The relation between the velocity at the contact point and the linear and rotational velocities at the pseudo-center is given by equation (4) approximately. Consequently, if the velocity at the contact point ${}^{U}\mathbf{V}_c$ is settled as:

$${}^{O}V_c=\mathbf{B}^{-1}\left[\bar{v}_0,\dot{q}\right]^T,$$
$$\mathbf{B}=\begin{bmatrix}\cos a_0 & \sin a_0\\ \frac{1}{l_p}\sin a_0 & -\frac{1}{l_p}\cos a_0\end{bmatrix} \tag{5}$$

it can be expected to make the object follow the desired trajectory. The control variable, that is, the manipulator tip velocity ${}^{U}\mathbf{V}_c$ realizing the above ${}^{O}V_c$ is given by:

$${}^{U}V_c={}^{U}\mathbf{R}_0\,{}^{O}V_c. \tag{6}$$

2. Force sensing for micro handling

If excessive contact force is applied to small objects which are light and fragile, they can flip away or be broken easily. A force sensor should therefore monitor the minute micromanipulation force during handling operations. A specific micro end-effector integrating a buckling-type force sensor has been developed and settled at both end-effectors [14]. The proposed force measurement methodology is based on a non-contact technique. More precisely, it consists to measure the out-of-plane bending deflection of the end-effector by an optical measurement system. When a normal pushing force is applied to the end-effector, the stress on the flexible buckling beam results in an out-of-plane deflection. The amplitude measured on the top of the buckling beam is used to measure the magnitude of the applied force at the contact interface between the object and both manipulators. In our analysis, we consider as a first approximation, that the sensor is a beam of finite length clamped at the ends and linearly elastic. Here, we have considered that the compression load is applied at one end of the beam.

The out-of-plane deflection displacement z at any point is given by the following fourth order differential equation:

$$EI\frac{\partial^4 z}{\partial x^4}+F\frac{\partial^2 z}{\partial x^2}=0, \tag{7}$$

where: EI = flexural rigidity of the beam, F = compression load. The boundary conditions are :

$$z(0)=z(L)=0\ ;\ \frac{\partial^2 z}{\partial x^2}(0)=\frac{\partial^2 z}{\partial x^2}(L)=0. \tag{8}$$

The solution for the above differential gives the variation of the out-of-plane displacement (Fig.5) for several ratio $k=h/L$ of the beam geometry. These results show clearly that the deflection increases gradually with the compression load until to reach the critical load, F_C, at the origin of the buckling of the beam. It can expressed by :

$$F_C=\frac{4p^2EI}{L^2}. \tag{9}$$

Close to the buckling zone, the force sensor is strongly nonlinear. Furthermore, the variation of the parameter k influences the sensor accuracy and sensibility. In order to increase the performances of the sensor in the linear zone by reducing its structural rigidity, the parameter k must be chosen as high as possible. For more information, the reader may refer to

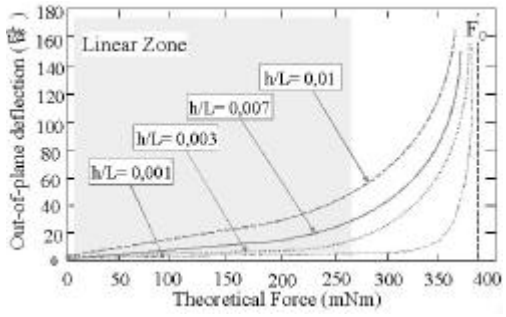

Fig. 5. Theoretical results of the deflection for different beam stiffness values ($k=h/L$).

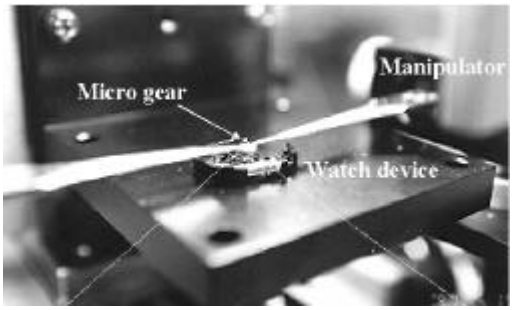

(a)

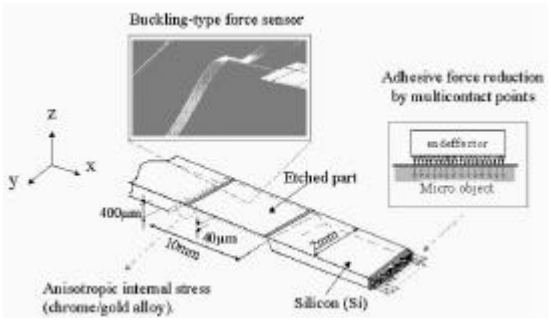

(b)

Fig. 6. (a) Picture of the micro-handling operation, (b) geometry of the micro-endeffector with integrated buckling-type force sensor and multi-contact points adhesive force reduction.

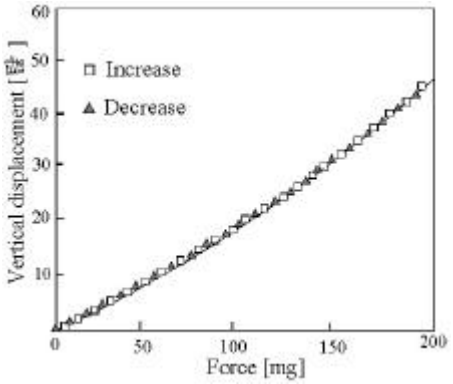

Fig. 7. Calibration of the integrated force sensor.

[14]. The detail drawing of the proposed end-effector design is shown in Fig. 6(a). In the design of the end-effector, we have to consider also that the surface tension forces are dominant for object dimensions ranging from several hundred micrometers to few millimeters. We adopted a multi-contact geometry of the end-effector's tip for adhesive force reduction. Polysilicon micro-contacts have been realized by etching process and glued onto the end-effector's tip surface.

- *Calibration of the sensor:* At the tip of the end-effector, we applied force by high-precision mechanical loading system –constituted by a stylus loaded with a piezoelectric table through the control of a weighting machine–. The bending deflection is measured at point where the vertical deflection is maximum by an optical interferometer apparatus. From these measurements, it is thus possible to calibrate precisely the applied force. Experimental results (Fig. 7) shows that the force sensor presents good performances (linearity, sensibility and accuracy) in the linear behavior of the end-effector structure. Hysteresis is negligible owing to the elastic properties of the silicon material. Accuracy of this force sensor is less than few 10^{-3} gf order. We can improve its accuracy by reducing the structural rigidity of the prototype end-effector.

- *Graphic image processing of deformation shape :* After the calibration procedure realized through an optical interferometer, bidimensional deflection measurements of the elastic structure is investigated in this paragraph in order to estimate the contact forces. The gray-level data vizualized through the optical microscope and acquired by the high-definition CCD camera are sampled by the video frame grabber. The data are then transferred to the workstation. We have to take into account several problems related to graphic image processing of the deflection distribution.

First, the distorsion problem cannot be neglected because we observe the task at a relatively low magnification ratio of 1,400. It can be noticed at the circumferential part in the field of view. Therefore, the left and right sides of the image are cut away in order to keep the central area. Images issued from the optical microscope are generally noisy. Noise reduction is implemented by applying a Gaussian filter. This filter reduces the sharpness of the image but donot affect image recognition and definition performance. Detection of edges from smoothened images is then initiated. The number of detected edges are limited to the sensing part (rectangular shape). It allows to do not degrade the reliability and speed of the optical image processing since the structure shape is quasi-static.

Afterwards, from the sampled image data of the buckling-type force sensor, the gray-level distribution of the out-of-plane beam deflection is calculated. However, the visual control of the beam deflection give information about qualitative but not quantitative displacements. Precise quantization of the micrometric out-of-plane deflection acquired by the vision system is realized using the calibrated data. Figure 8(a) shows experimental bidimensional distribution of the vertical displacement for two values of force contact. A three-dimensional graphic representation (Fig.8(b)) is reconstructed. In order to obtain the smooth wire-frame curve line from small numbers of sampled data, a cubic Spline function was applied.

Based on the deformation shape of the force sensor the operator can detect instabilities of the micro handling operation by analysis of the force homogeneity along the buckling beam. The guiding-based visual feedback allows the operator to

monitor and to supervise on-line the mechanical stability of the different handling and manipulation tasks.

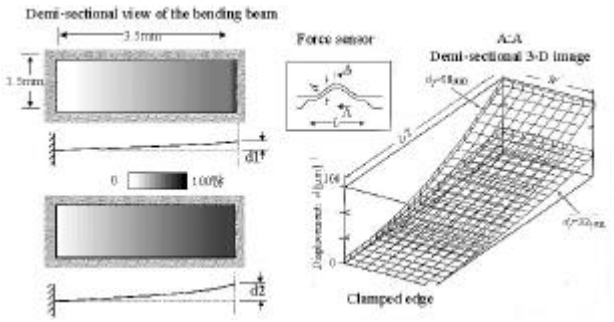

Fig. 8. Deformation shape of the force sensor: (a) demi-sectional views of the 2-D displacement distribution of the force sensor for d_1=32μm and d_2=98μm; (b) 3-D graphic image of the resultant bending deflection.

IV. Results from integrating visual force and position feedback

1. Visual position and force feedback loop

Figure 9 presents the strategy adopted for integrating force and position feedback. It is imperative to use a such vision system for the following reasons [15]: 1) as mentioned above, most of the d.o.f. have a good resolution but a poor repeatability, 2) during the pushing operation, friction forces at the micro-object/support interface induces errors in the orientation and positioning of the micro-object which implies the use of a vision-based position control system, and 3) to control the contact force at the micro-object/manipulator tip interfaces, a vision-based force sensor is required. For highly accurate manipulations the parameters describing the relationship between the image frame and the frame attached to manipulators must be continuously and accurately updated. These parameters are unknown a priori and are not directly measurable, but can be deduced by observing the scene change during motion. Because our simple vision system does not process images in real time, the algorithm is based on a ‘ ’look and move’ ’ strategy, i.e. the motion is realized in steps, during which the manipulators and the worktable are controlled in a closed-loop. In addition, we calculate predictions of pattern positions on-line

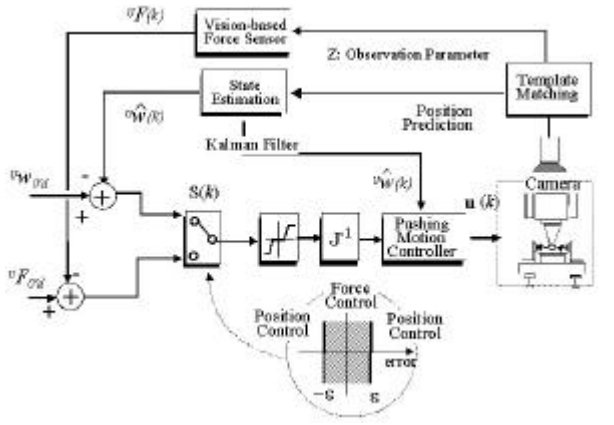

Fig. 9. Diagram of visually servoed position and force feedback.

for. optimal trajectory control. This is done using an Extended Kalman Filter (EKF). The two inputs are the desired state of visual features observed by the optical microscope, ${}^{U}w_{0'd}$, and the desired contact force at the object/tool interfaces, ${}^{U}\boldsymbol{F}_{0'd}$. The desired feature state represents visual features of the object upon to initiate the micro handling operation. When the error vector in visual features $e_{0'} = \left[{}^{O'}\mathbf{p}_e{}^{T}, q_e\right]^{T}$ is large, the switching controller *S(k)* uses pure vision feedback to control the position object according to Eq. (4). When the error vector is less than a threshold value ε, the handling operation can be initiated by switching the controller *S(k)* to the vision-based force control feedback. The object is handled and maintained in a stable way when the desired contact force ${}^{U}\boldsymbol{F}_{0'd}$ is reached. The switching controller is described by the following law :

$$\text{for } \left|{}^{U}\mathbf{p}_{0'd} - {}^{U}\mathbf{p}_{0'}\right| > e \quad \text{then}$$

$$u(k) = J(k)^{-1} M(k)^{-1}.\left({}^{U}w_{0'd} - {}^{U}\hat{w}\right)$$

$$= J(k)^{-1} M(k)^{-1}.\begin{bmatrix} \bar{\mathrm{v}}_{0'd}(k).\cos q_e(k) + K_x{}^{0'}\mathrm{x}_e(k) \\ \dot{q}_d(k) + \bar{\mathrm{v}}_{0'd}(k).\left(K_y{}^{0'}\mathrm{y}_e(k) + K_q \sin q_e(k)\right) \end{bmatrix}$$

$$\text{else } \left|{}^{U}\mathbf{p}_{0'd} - {}^{U}\mathbf{p}_{0'}\right| \le e \text{ and } \left|{}^{U}\mathbf{F}\right| \ge F_H \text{ then}$$

$$u(k) = J(k)^{-1} M(k)^{-1}.\left({}^{U}\mathbf{F}_{0'd}(k) - {}^{U}\mathbf{F}(k)\right)$$

The terms F_H, M and J are force threshold value, scaling factors of the command signals (m_x, m_y, m_q) and the Jacobian matrix of the micromanipulators, respectively. The output of the controller *u(k)* is a velocity command that is sent to the piezoelectric micromanipulators. Practically, the greater each motion step from one image to the next, poorer is the parameter estimation predictions. It can be explained by the fact that the estimation of the pattern which is expected to be observed in the next image becomes uncertain. It led us to use small incremental steps for the servoed position and force feedback.

2. Micro positioning results

In the simulation, the object is assumed to have a silicon rectangular base with 5×3×2 [mm], and have a friction distribution uniform. The silicon support is mirror-finished in order to facilitate the motion guidance. We want to move this object from ${}^{U}\mathbf{p}_{0'd}(0)=[2,0]^{T}$ ([mm], [mm]), $\theta(0)_d = 0$[deg] to ${}^{U}\mathbf{p}_{0'd}(15)=[0,30]^{T}$ ([mm], [mm]), $\theta(15)_d=0$[deg] in the time interval of 15 seconds. The contact is the foot of the perpendicular from the center of friction to the side of the object. It is assumed that there is no slip or detachment at the end-effector/object interface. The coefficient of friction at the contact point is assumed to be μ=0.3 in the simulation. Note that the simulation described before is the case that the manipulator tip velocity lies in the velocity cone. Then, to observe the convergence of the errors with respect to the desired position and trajectory, we have chosen the feedback parameters as K_x = 18, K_y=66 and K_θ= 15 (critical damping case). The Fig. 10(b) shows a result of simulation. As can be seen from the figure, the actual trajectory converges to the desired one quickly. This result shows the effectiveness of the proposed control method. Experimental results are shown in Fig. 10(c). In the Fig. 10(a), the desired trajectory of the reference point is shown by the dotted line and its actual trajectory is shown by the solid line. The rest information is shown in the same way

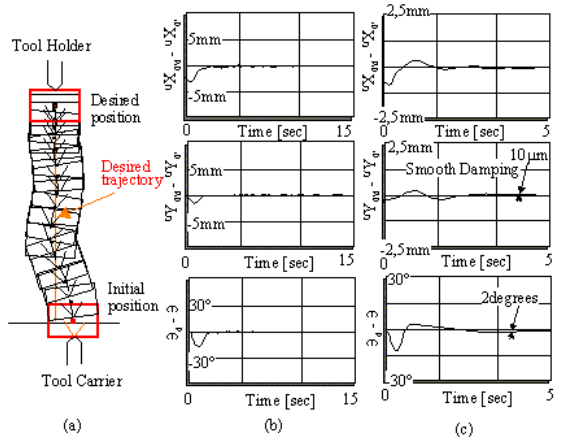

Fig. 10. (a) Experimental results of position and trajectory tracking, (b) simulation and (c) experimental of tracking errors.

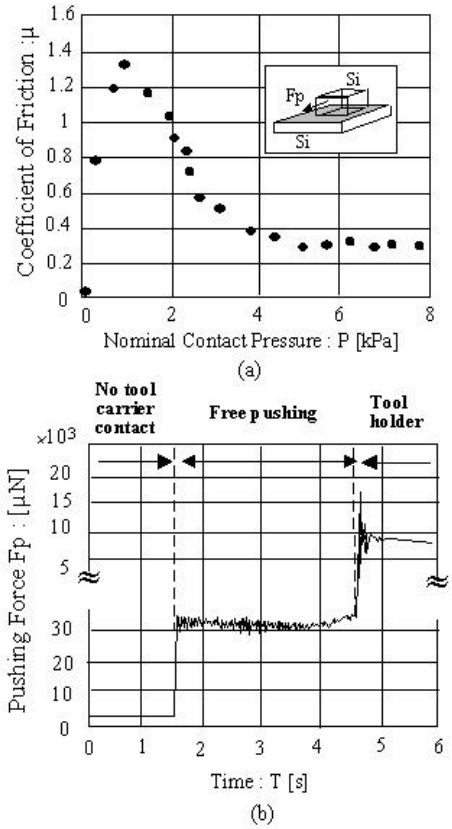

Fig. 11. (a) Experimental coefficient of friction and (b) pushing force during trajectory control.

as Fig. 10(c). Experimental results have shown that the object follows the desired trajectory in xy coordinates with good performance, i.e., typical error values ($^{U}\mathbf{x}_{0'd}$- $^{U}\mathbf{x}_{0'}$) and ($^{U}\mathbf{y}_{0'd}$- $^{U}\mathbf{y}_{0'}$) are less than 10μm although the tracking performance of the orientation is slightly degraded; i.e. ($\mathbf{q}_d$- $\mathbf{q}$) <2 degrees. The smooth damping and error position are due to the fact that the actual friction distribution is supposed to change according the movement of the object due to the surface forces at the object/support interface. When contact pressure is low, the coefficient of friction tends to become large as shown in Fig.11(a). This phenomenon is well known in the microscale taking into account attractive force between the surfaces (electrostatic, meniscus, and son on). One way to reduce the coefficient of friction improving the frictional directionality of motion guidance is to use textured shape at the contact region. It will suppresses the increase of friction in the low-contact pressure region. Fig.11(b) shows the result of controlled pushing operation. In practice, it has been observed that any slip between the object and the manipulator tip occurred which proves that the direction pushing velocity lied in the velocity cone.

3. Micro handling results

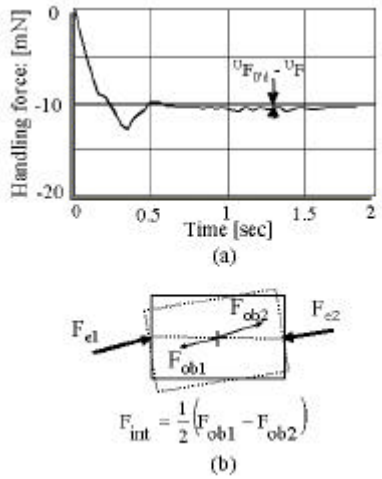

Fig. 12. (a) Experimental results of handling force tracking, and (b) force parameter of cooperative control system.

To test the performance of the handling task, the response of the force control is shown in Fig.12. The generated handling force using the proposed control scheme tracks the desired handling force. This is indicated by the maximum handling error (Fig.12(a)) which is in the order of ($^{U}\mathbf{F}_{0'd}$-$^{U}\mathbf{F}$)<1.5mN. During this experiment, the micromanipulators are controlling the orientation of the handling vector forces while keeping the object position in order to keep the exerted forces (F_{e1}, F_{e2}) and the internal force F_{int} always mutually linear. In some cases where the handling forces are so large, it was difficult for the system to keep the stability of the handled object, and causes undesirable state which result in breaking or dropping the object.

V. Microassembly supervision through a virtual reality interface

A task-based teleoperation approach has been investigated where the operator determines the tasks to be performed, and a controller realizes these tasks automatically with the aid of a virtual reality (VR) guiding-system interface.The combination of vision servoing techniques and VR-based simulation system allows to plan the manipulation tasks and to insure the guided-movements of the micromanipulators preventing any collisions, and also increasing safety and reliability of the distributed assembly workcell. In our system, a VR-teleoperator interface giving a 3-D map of the scene (Fig.13) is provided to

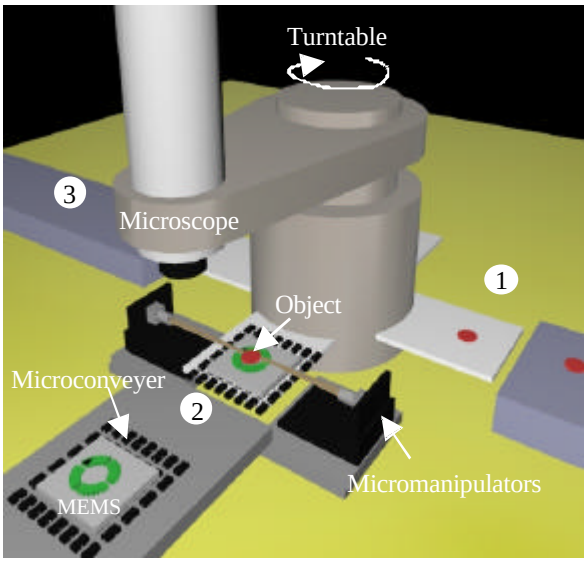

Fig. 13. VR-interface describing the distributed assembly workcell in the micro world.

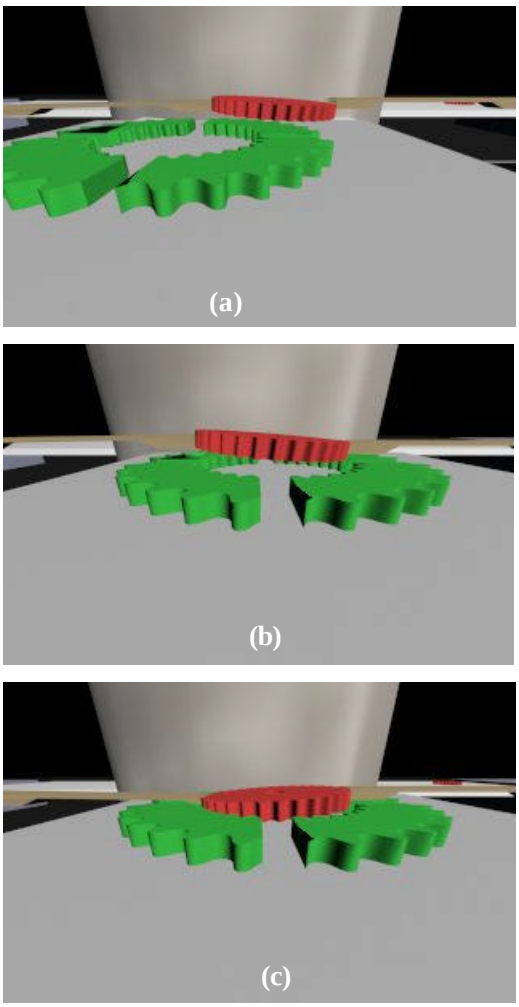

Fig. 14. Programmed task during the positioning (a) and (b-c) the insertion of a micro planetary gear.

the user for semi-automatic positioning sequences in an absolute frame. It describes the sequencing of the different workstations: (1) feeding workcell providing micro-objects, (2) positioning, handling and assembly workcell and (3) transportation of the MEMS. devices. These production units are functionally combined with conveyance systems in order to perform complicated tasks such as transportation, positioning or alignment of micro-objects. The small field of view of the microscope implies that small portion of the working area only can be seen at the same time. For that the user can chose between a global 3D-view of the entire system or a closed 2D-view of the microdevice through a virtual optical microscope by zoom-in. The operator is immerged into the virtual scene exactly reconstructed from CAD-CAM databases of the real micro-world environment. The pictures (a) to (c) shown in Fig.14 illustrate the procedures followed in planning the different trajectories for the assembly task of the outer and inner parts of a micro planetary gear.After acceptation of the simulation, the treated information in the virtual world is sent to the assembly execution planner. Figure 15 shows the real micro world view of the assembly task from the OM. Since the micro gear component to be assembled has to be carried from a distant location, a map of the whole working area delimited by the MEMS device, is provided to the user. The handled object is moved automatically under vision control to the specified location. Three passing points have been planed. First, the microrobot is driven automatically toward the first passing point. Its movement is coarsely controlled by vision feedback. This procedure stops when the object has been reached the goal position with the user's accuracy. Then, the alignment operation is initiated by controlling accurately the cooperative movements of both piezoelectric microconveyer and micromanipulators. A matching algorithm allows to achieve an alignment accuracy of 300nm between the outer radius of the micro axle and the inner radius of the micro-gear. Finally, the insertion operation is thus possible. However, to improve the insertion procedure, operation information of 3-D object location is required. The concentration of the fields of view of the microscope and an additional camera located perpendicularly to the latter, will allow to perform an accurate 3-D object location in the same working space.

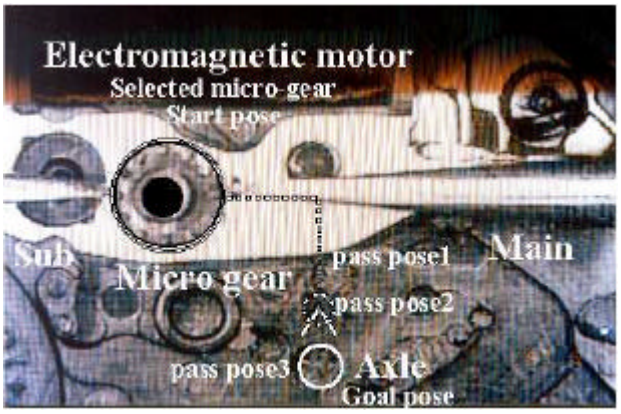

Fig. 15. Closed-view of the planned assembly task of a gear hole in a desired axle: transportation (pass pose1), alignment (pass pose2), and insertion (pass pose3).

VI. Conclusions

The goal of our project is to assemble automatically complex hybrid MEMS devices through visual teleoperated micro-manipulation. The first results presented in this paper related to the integration of enhanced techniques of visual servoed techniques and real time 3D computer graphics(Virtual Reality) shows the possibility to develop integrated micro assembly stations. Work is being undertaken to improve the vision system and the VR-teleoperator interface in order to ensure the total guidance of the micro-object from the handled task to the transportation. More work will also be investigated in order to implement new end-effectors dedicated to other micro-manipulation tasks.

References

[1] A. Codourey, M. Rodriguez, I. Pappas, "A task-oriented teleoperation system for assembly in the micro-world," *Proc. of International Conf. on Advanced Robotics*, Monterey, USA, 1997.

[2] A. Sulzmann, J-M. Breguet, J. Jacot, "Microvision system (MVS): a 3D computer graphic-based microrobot telemanipulation and position feedback by vision," *SPIE Conf. on Microrobots and Micromechanical Systems*, Philadelphia, PA, USA, 1995.

[3] S. Fatikow, R. Munassypov, U. Rembold, "Assembly planning and plan decomposition in an automated microrobot-based microassembly desktop station," *Journal of Intelligent Manufacturing*, **9**, pp. 73-92, 1998.

[4] H. Ishihara, T. Fukuda, K. Kosuge, F. Arai, K. Hamagishi,"Approach to distributed micro robotic system – development of micro line trace robot and autonomous micro robotic system," IEEE Int. Conf. On Robotics and Automation, 1995.

[5] H. Aoyama, F. Iwata, A. Sasaki, "Desktop flexible manufacturing system by movable miniature robots – miniature robots with micro tool and sensor," *IEEE Int. Conf. On Robotics and Automation*, pp.660-665 (1995).

[6] A. Ferreira, S. Hirai, "Cooperative micro object handling by dual micromanipulators under vision control," 13th IFTOmm Symposium on ROMANSY, Zakopane, Poland, 2000.

[7] A.Ferreira, "Design and control of a mobile micromanipulator driven by ultrasonic motors with multidegrees of freedom," *Journal of Advanced Robotics*, vol.12, no.2, pp.115-133 , 1998.

[8] A. Ferreira, "Design of a flexible conveyer microrobot with electromagnetic field-based friction drive control for microfactory stations," J. of Micromechatronics, vol.1, no.1, pp. 49-67, 2000.

[9] A. Ferreira, J-G. Fontaine, "Coarse/Fine motion control of a teleoperated autonomous piezoelectric nanopositioner operating under a microscope," *IEEE/ASME Int. Conf. on Advanced Intelligent Mechatronics*, Como, Italy, pp. 1633-1639, 2001.

[10] C.Cassier, A. Ferreira, S. Hirai "Combination of vision techniques and VR-based simulation for semi-autonomous microassembly workstation," *IEEE Int. Conf. on Robotics and Automation*, Whashinton, DC (2002).

[11] W.Zesch, R.S. Fearing "Alignment of microparts uisng force controlled pushing," *SPIE Conf. on Microrobotics and Micromanipulation*, Boston, MA, pp.148-156 (1998).

[12] J.A. Thompson, R.S. Fearing "Automating microassembly with ortho-tweezers and force sensing," *IEEE/RSJ Int. Conf. on Intelligent Robots and Systems*, Hawai, USA, pp.1327-1334, 2001.

[13] M. Kurisu, T. Yoshikawa, "Tracking control for an object in pushing operation," *Proc. IEEE IROS*, 1996, pp.729-735.

[14] A. Ferreira, J-G. Fontaine, "New vision-based flexible force sensor for micro-teleoperation systems," *XVI IMEKO World Congress*, Sep.25-28, Vienna, Austria, pp. 101-106, 2000.

[15] Y. Zhou, B-J., Nelson, B. Vikramaditya, "Fusing force and vision feedback for micromanipulation," *IEEE Int. Conf. on Robotics & Automation*, Leuven, Belgium, 1998.

Antoine Ferreira

He received the MS, PhD in Electrical and Electronics Engineering from the University of Franche-Comté (France) in 1993, 1996 respectively. In 1997 he was a Visiting Researcher at the ElectroTechnical Laboratory (ETL), in Tsukuba (Japan). He is currently a Associate Professor at the Laboratoire de Vision et Robotique of Bourges (France). His main research interests are focused on the design, modeling and control of microrobotic systems using active materials and micro-nano-teleoperation .

Jean-Guy Fontaine

He received MS, PhD degree in electrical engineering. He is currently professor at the Laboratoire de Vision et Robotique of Bourges (France). He is also research director of Ecole Nationale Supérieure d' Ingénieurs of Bourges. His research works are focused in teleoperation, telepresence and teleexistence with mobile and static robotic systems.

Shigeoki Hirai

He is Deputy Director, Intelligent Systems Institute, Advanced Industrial & Science Technology (AIST). He received the BS, MS and PhD from Tokyo Institute of Technology in 1973, 1975, and 1978, respectively. Since 1978 he had been with Electrotechnical Laboratory, MITI, Japan. The Electrotechnial Laboratory has been reorganized as a part of National Institute of Advanced Industrial & Science Tehnology (AIST) April 2001. His research works include expert systems, advanced and intelligent telerobotic systems, and man-robot interfaces. Currently he works as Deputy Director of Intelligent Systems Institute, AIST